Climate Dynamics (2019) 53:4611–4627
https://doi.org/10.1007/s00382-019-04812-2

Performance of a high resolution regional ocean–atmosphere coupled model over western North Pacific region: sensitivity to cumulus parameterizations

Liwei Zou[1,2] · **Tianjun Zhou**[1,2] · **Hailong Liu**[1]

Received: 8 December 2018 / Accepted: 8 May 2019 / Published online: 18 May 2019

Abstract
In this study, we developed a high-resolution regional ocean–atmosphere coupled model, based on RegCM4 and a North Pacific Ocean model, through the OASIS3 coupler. The horizontal resolution of the atmospheric component (oceanic component) was set to 15 km (0.1°). With the motivation to customize the model over western North Pacific (WNP) region, the sensitivity to three cumulus parameterization schemes (MIT-Emanuel, Tiedtke, Kain–Fritsch) was investigated with the focus on the WNP summer monsoon of 2005. The results indicated that a simulation with the Tiedtke scheme exhibited the relatively best performance over this region in terms of sea surface temperature (SST), rainfall, and circulation. Fifty percent of the model grids had biases of SST (rainfall) within ± 0.5 °C (± 2 mm/day) over WNP. In addition, the simulation with the Tiedtke scheme reasonably captured the shape and magnitude of the monsoon trough rainfall, the northward movement of the rainband and the associated circulation changes over WNP. However, the apparent heat source (Q_1) and moisture sink (Q_2) in the simulation with the MIT-Emanuel (Kain–Fritsch) scheme were nearly half (double) those of the observed measurements, especially in the lower troposphere over the monsoon trough region. The too weak (too strong) diabatic heating favored a weaker (stronger) ascending motion, which led to the underestimation (overestimation) of vertical moisture advection over the monsoon trough, thus resulting in evident dry (wet) biases. Our analysis suggested that the improved performance using the Tiedtke scheme could be attributed to the improved simulated vertical profile of diabatic heating, the inclusion of the effects of large-scale forcing in the cumulus parameterization, and the reasonable simulated relationship of precipitation with low-level vertical velocity.

Keywords Regional climate modeling · Regional air–sea coupling · Cumulus parameterizations

1 Introduction

Regional climate models (RCMs) with better-resolved local terrain and surface characteristics have been widely used as a useful tool for a wide variety of applications, including for regional climate studies and future regional climate projections (Giorgi and Mearns 1999; Leung et al. 2003; Wang et al. 2004; Christensen et al. 2007). The Coordinated Regional Downscaling Experiment (CORDEX), one of the major international programs within the regional climate modeling community, aims to improve downscaling techniques and to provide reliable high-resolution climate information for impacts and adaptation studies (Giorgi et al. 2009; Jones et al. 2011; Gutowski et al. 2016).

One of the frontiers in regional climate modeling is the coupling of other components of the climate system at the regional scale (Giorgi and Mearns 1999; Gutowski et al. 2016). Coupling of the ocean component in RCMs has already been conducted with a focus on many regions of the world. One of the research foci employing a regional ocean–atmosphere coupled model is the Asian summer monsoon (Zou and Zhou 2016) and its subcomponents, including the South China Sea monsoon (Lu et al. 2000), the East Asian monsoon (Ren and Qian 2005; Yao and Zhang 2010; Li and Zhou 2010; Fang et al. 2010; Cha et al. 2016;

✉ Liwei Zou
zoulw@mail.iap.ac.cn

[1] LASG, Institute of Atmospheric Physics, Chinese Academy of Science, Beijing 100029, China

[2] CAS Center for Excellence in Tibetan Plateau Earth Sciences, Chinese Academy of Sciences (CAS), Beijing 100101, China

Dai et al. 2018), the Indian monsoon (Ratnam et al. 2009; Seo et al. 2009), and the western North Pacific monsoon (Zou and Zhou 2011, 2012, 2013). The negative correlation between the observed sea surface temperature (SST) and precipitation over the Asian summer monsoon region highlights the importance of local air–sea interactions in the simulation of the climatology and interannual variability of the Asian summer monsoon (Wang et al. 2005; Kumar et al. 2005; Zhou et al. 2009). The comparisons between the coupled and uncoupled regional climate simulations indeed show that summer monsoon rainfall and circulation were better simulated in the regional coupled simulation, although overall cold biases of the SST are simulated (e.g., Ratnam et al. 2009; Li and Zhou 2010; Zou and Zhou 2013; Zou et al. 2016).

These above studies were mainly based on regional ocean–atmosphere coupled models with a horizontal resolution of 30–60 km for both atmospheric and oceanic components. This kind of horizontal resolution is currently considered coarse to some extent. First, to well represent topographic effects on climate change, the resolution of the RCM should be at least 10–20 km (Giorgi et al. 2016). Second, to well resolve ocean mesoscale eddies, the horizontal resolution of the ocean model should be approximately 10 km. A recent study indicated that the feedback between ocean mesoscale eddies and the atmosphere is fundamental to the dynamics and control of the strong western boundary currents (Ma et al. 2016). In this regard, it is necessary to develop a regional ocean–atmosphere coupled model with a horizontal resolution of approximately 10–20 km for climate studies over the Asian monsoon region.

Cumulus parameterization is crucial to regional climate models with a horizontal resolution of 10–20 km (Arakawa 2004). There are various cumulus parameterization schemes with different closure assumptions and convection trigger mechanisms. The selection of an appropriate cumulus parameterization scheme is usually the first step for customization of an RCM over a target region. The newly developed RegCM4 (Giorgi et al. 2012) at the Abdus Salam International Centre for Theoretical Physics (ITCP), for example, has been customized for many regions of the world. Martinez-Castro et al. (2018) investigated the sensitivity of RegCM4 to different cumulus parameterizations over the Central America and Caribbean regions. They found that the configuration with the Tiedtke cumulus scheme shows the most balanced range of biases across variables. Gao et al. (2016) compared the performance of RegCM4 with different convective parameterizations over China. They recommended the Emanuel cumulus scheme for future applications. Raju et al. (2015) investigated the sensitivity of RegCM4 to different convection schemes over South Asia and found that a mixed scheme (Emanuel over land and Grell over the ocean) is optimal. For Southeast Asia, Lui et al. (2018) conducted similar work but recommended the Emanuel scheme with some modifications of the trigger mechanisms. It is noted that nearly all the aforementioned studies were based on the uncoupled RegCM4, although some of the simulated domains covered large portions of the ocean. Therefore, the sensitivity of the ocean-coupled RegCM4 to cumulus parameterizations warrants further investigation.

In this study, we develop a high-resolution regional ocean–atmosphere coupled model based on RegCM4 and a North Pacific Ocean model. The horizontal resolution of the atmospheric component is set to 15 km, while that of the oceanic component is 0.1°. The regional ocean–atmosphere coupled model is applied to the western North Pacific monsoon region. Three 1-year simulations with different cumulus parameterization schemes are conducted. The objectives of this study are as follows: (1) to introduce the developed regional coupled model and assess the model's performance over the Western North Pacific; and (2) to investigate the sensitivity of the regional ocean–atmosphere coupled model to convective schemes and to explore the underlying mechanisms, with particular interest over the monsoon trough. Our results indicate that the regionally coupled simulation with the Tiedtke scheme exhibits optimal performances over this region, especially over the monsoon trough, mostly because it reproduces the vertical profile of diabatic heating well, takes into account the effects of large-scale forcing in cumulus parameterization, and reasonably simulates the relationship of the low-level vertical velocity with precipitation.

The remainder of the paper is organized as follows: the models, the experimental design and the observational datasets are described in Sect. 2. The sensitivity of the simulated SST, rainfall and circulations to cumulus parameterization schemes are presented in Sect. 3. Section 4 discusses the underlying mechanisms of why the regionally coupled simulations differ remarkably over the monsoon trough. The major results and concluding remarks are summarized in Sect. 5.

2 Model description, experimental design, and observational datasets

2.1 Regional ocean–atmosphere coupled model

2.1.1 Atmospheric model component

The atmospheric model component of the regional ocean–atmosphere coupled model is the RegCM4 model (Giorgi et al. 2012) version 4.6, which was developed at ICTP. It is a limited area model, with a hydrostatic dynamical core and a terrain-following sigma vertical coordinate system. The following model physics are employed: the community land model (CLM) 3.5 (Oleson et al. 2008),

the subgrid explicit moisture scheme (Pal et al. 2000), the radiation package of the NCAR community climate model version 3 (Kiehl et al. 1996), the nonlocal vertical diffusion scheme of Holtslag et al. (1990) with some modifications (Giorgi et al. 2012), and the ocean–atmosphere flux algorithm proposed by Zeng et al. (1998).

The RegCM4.6 includes several options for the cumulus parameterization scheme. In this study, we investigate the sensitivity of the regional ocean–atmosphere coupled model performances to three cumulus parameterizations. The first is the MIT-Emanuel scheme (Emanuel 1991; Emanuel and Rothman 1999), in which the convection is triggered when the level of neutral buoyancy is higher than the cloud base level. In the MIT-Emanuel scheme, mixing in clouds is assumed to be highly episodic and inhomogeneous, and the mixing entrainment and detrainment rates are functions of the vertical gradients of buoyancy in clouds. The second is the Tiedtke parameterization (Tiedtke 1989; Nordeng 1994). In the Tiedtke scheme, a one-dimensional model represents the cloud ensemble and both updraft and downdraft are included. Updraft interacts with the environment through convective entrainment and detrainment. Three types of convection are considered. The deep penetrative convection and midlevel convection are produced by large-scale moist convergent flow, while shallow convection is maintained by the supply of moisture due to the surface evaporation. The third is the Kain–Fritsch scheme (Kain and Fritsch 1993; Kain 2004). The Kain–Fritsch scheme was operated by identifying the updraft source layer. When it is identified, the updraft flux is initialized with a velocity based on atmospheric instability and grid scale vertical motion. The entrainment and detrainment between the updraft and the environment occur at each layer.

2.1.2 Oceanic model component

The oceanic model component is a North Pacific Ocean model, which is the regional version of a quasi-global (excluding the Arctic Ocean) eddy-resolving ocean general circulation model (OGCM) (Yu et al. 2012). This eddy-resolving OGCM has been used to investigate the ocean mesoscale structure-induced air–sea interaction in a high resolution coupled model (Lin et al. 2019). This model was developed based on the global climate ocean model, LICOM2 (LASG/IAP climate ocean model) (Liu et al. 2012), which has been employed as the oceanic component of the LASG/IAP global ocean–atmosphere coupled model FGOALS that participated in Coupled Model Intercomparison Project Phase 5 (CMIP5) (Li et al. 2013; Bao et al. 2013). The North Pacific Ocean model adopts the geographic longitude–latitude grid and η coordinates in the vertical. A second order closure turbulence model (Canuto et al. 2001, 2002) is used to parameterize the vertical mixing process due to the velocity shear and the internal-wave break. The North Pacific Ocean model is referred to as "LICOM_np" in the following discussion.

2.1.3 Ocean–atmosphere coupling

Ocean–atmosphere coupling is accomplished through the OASIS3 (Ocean Atmosphere Sea Ice Soil, version 3) coupler (Valcke 2006). During the coupling, RegCM4 provides the sea surface heat flux and wind stress to LICOM_np, while LICOM_np supplies the sea surface temperature (SST) field and ocean surface current to RegCM4. The relative motion of surface wind and ocean surface current is taken into account in the calculation of the sea surface turbulent heat flux and wind stresses since some observational and modeling studies have demonstrated the importance of surface ocean currents in the estimation of surface wind stress curl fields (Chelton et al. 2004; Luo et al. 2005).

2.2 Experimental design

The model domain of RegCM4 is set to the western North Pacific region (dashed region of Fig. 1) with a uniform horizontal resolution of 15 km. There are 23 sigma layers in the vertical direction, with the model top at 10 hPa. The buffer zone of RegCM4 is 20 grid layers. The initial and lateral boundary conditions are derived from the European Centre for Medium-Range Weather Forecasts (ECMWF) interim reanalysis (ERAIM hereafter; Dee et al. 2011) with a horizontal resolution of $0.75° \times 0.75°$, which is updated every 6 h.

LICOM_np is a North Pacific Ocean model that covers 98°E–74.9°W, 10°S–66°N (shaded region of Fig. 1). The horizontal resolution of LICOM_np is uniformly 0.1°. There are 55 vertical levels, with 36 uneven layers in the upper 300 m. The depth of the first layer is 5 m. The northern and eastern boundaries of LICOM_np are covered by land and are set to be rigid. In the southern open boundary (10°S) of

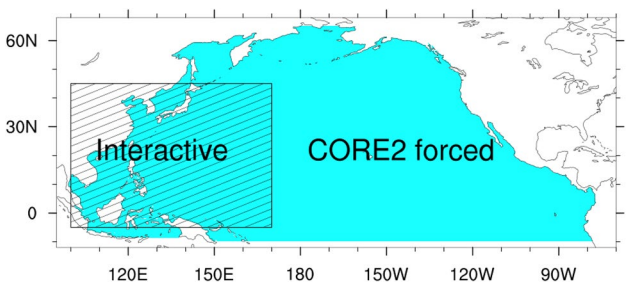

Fig. 1 Model configuration. The shaded (dashed) region is the regional oceanic (atmospheric) model domain. The oceanic and atmospheric components are fully interactive over the western North Pacific (dashed region), while the ocean model is driven by the CORE-II data outside the WNP

LICOM_np, the model temperature and salinity are restored to the climatological monthly temperature and salinity from the Levitus data (Levitus et al. 1994), while the solid wall boundary condition is used for velocity. Before the regionally coupled simulation, the LICOM_np model is forced by a 1-year repeating cycle of atmospheric forcing from the Coordinated Ocean-Ice Reference Experiment (CORE) for 30 years, with the initial condition of temperature and salinity from World Ocean Atlas 2005 (WOA05) (Locarnini et al. 2006; Antonov et al. 2006). Then, the model is forced by interannually varying atmospheric forcing derived from CORE phase II from 1990 to 2007. The LICOM_np model exhibits a reasonable performance over the western North Pacific region. The regional averaged June–July–August mean SST bias over the western North Pacific region (0–42°N, 105°–165°E) is quite stable (about − 0.2 °C) after 1997 (figure not shown). Figure 2 shows the spatial distribution of biases of simulated SST by LICOM_np averaged from June to August of 2005 over WNP. Cold biases of simulated SST are evident over North of 35°N with the largest biases (approximately − 2 °C) found over the Sea of Japan (Fig. 2), while the warm biases (approximately 0.5 °C) occurred over the region east of the Philippines and the Kuroshio Extension region.

The regionally coupled simulation begins on 1 November 2004. Over the oceanic area of the western North Pacific (WNP) region (dashed area of Fig. 1), RegCM4 and LICOM_np are fully interactive, with the coupling performed once per hour. However, outside of the WNP region, the ocean is forced by the daily atmospheric forcing from CORE-II. Therefore, the ocean subsurface within the coupling region is forced at the lateral boundaries by the surroundings of the rest of the ocean model, since the model domain of LICOM_np is larger than that of RegCM4. The regionally coupled model is integrated for 1 year, from Nov. 2004 through Nov. 2005. This modeling strategy follows Gao et al. (2016), who investigated the sensitivity of the RegCM4 model to different cumulus parameterizations over China through 1 year of simulations. In addition, the year 2005 is selected because the WNP summer monsoon is normal in that year (see Fig. 6 in Wang et al. 2008). In the following discussion, the regionally coupled simulations with the MIT-Emanuel scheme, Tiedtke scheme, and Kain–Fritsch scheme are referred to as "CPL_EM", "CPL_Tie", and "CPL_KF", respectively.

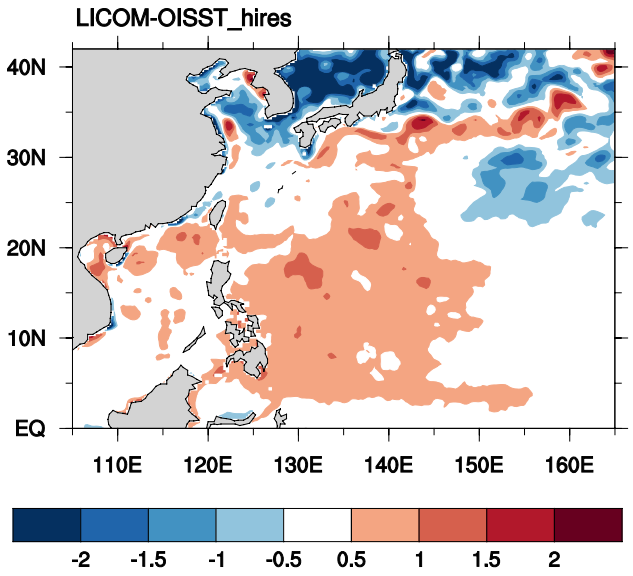

Fig. 2 Spatial distribution of the biases of the simulated SST (°C) by LICOM_np averaged from June to August 2005 over the WNP

2.3 Observational datasets

The following datasets are used to assess the model performance: (1) the resolution of the 0.25° satellite-retrieved precipitation dataset of the Tropical Rainfall Measuring Mission (TRMM) 3B42 (Huffman et al. 2007); (2) the daily mean circulation field (e.g., u, v, q) derived from ERAIM with a 0.75° × 0.75° grid; (3) the daily high resolution (0.25°) optimal interpolation sea surface temperature (OISST) data from the National Oceanic and Atmospheric Administration (NOAA) (Reynolds et al. 2007); (4) the surface solar and longwave radiation fluxes from Clouds and the Earth's Radiant Energy System (CERES) (Wielicki et al. 1996); (5) the sea surface latent and sensible heat fluxes derived from the objectively analyzed air–sea heat fluxes (OAFlux) version 3 (Yu et al. 2008). For simplicity, the rainfall dataset and the reanalysis-derived circulation dataset are referred to as "observation" in the following discussion.

3 Results

3.1 SST simulation

Figure 3 shows the observed and simulated SST, averaged from June to August of 2005, over the WNP region. The observed spatial pattern of SST is well reproduced in three regional coupled simulations, with spatial correlation coefficients (SCC) of 0.98, 0.98 and 0.97 for CPL_EM, CPL_Tie and CPL_KF, respectively. The CPL_EM and CPL_Tie simulations have lower root mean square error (RMSE) of simulated SST than the CPL_KF simulation, viz. 0.87 °C vs. 1.01 °C. Spatially, the cold (warm) biases of simulated SST over North of 35°N (Kuroshio Extension region), which are seen in the standalone LICOM_np simulation (Fig. 2), are also evident in the three regionally coupled simulations. The major differences of simulated SST among the three regionally coupled simulations are found over the South

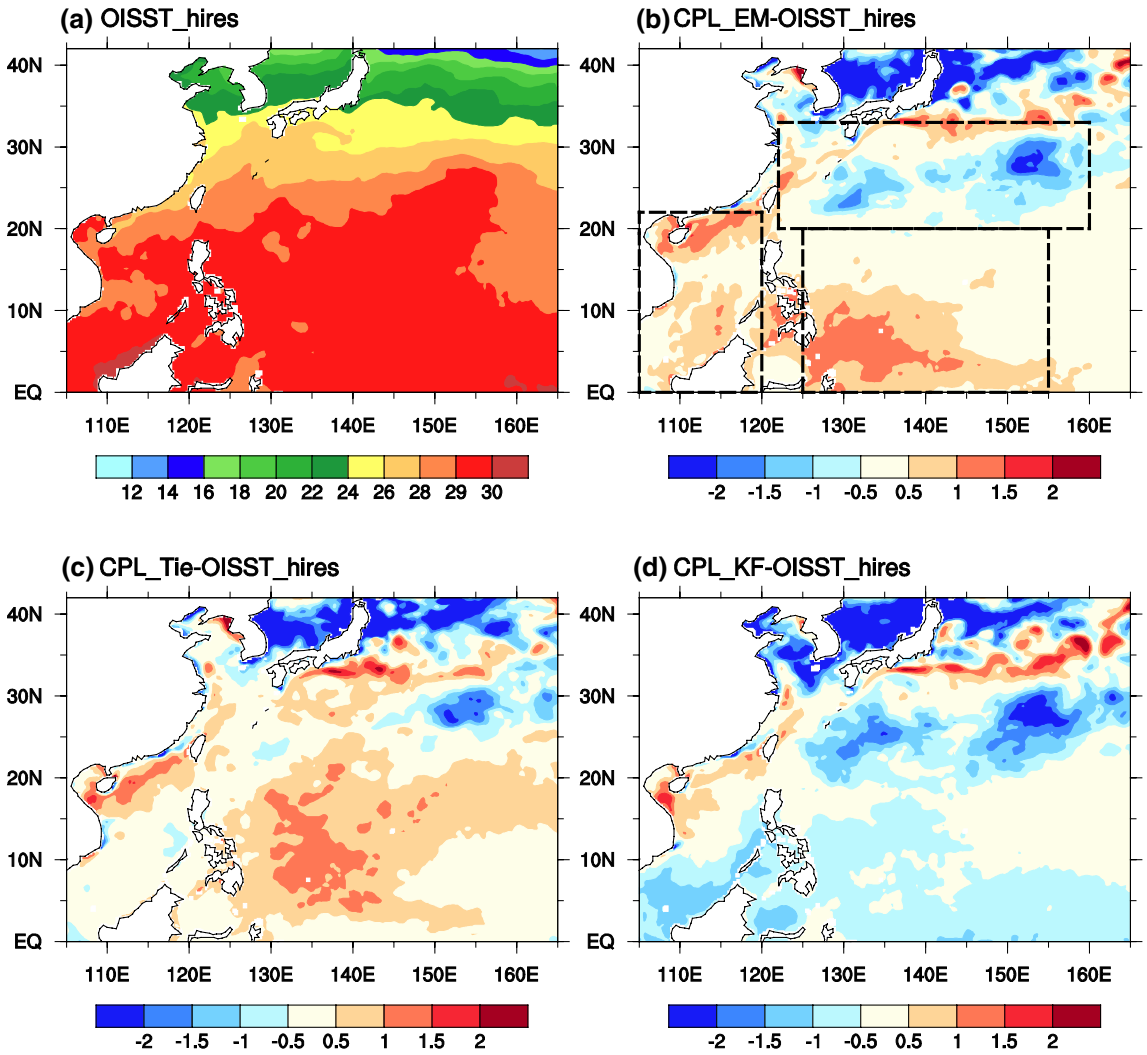

Fig. 3 **a** Spatial distribution of the SST (°C) averaged from June to August 2005 over the WNP from the observation. Spatial distributions of the simulated SST biases from **b** CPL_EM, **c** CPL_Tie, and **d** CPL_KF. The boxes (**b**) illustrate the three subregions: the South China Sea (0°–22°N, 105°–120°E), the east of the Philippines (0°–20°N,125°–155°E), and the subtropical region (20°–33°N, 122°–160°E)

China Sea, east of the Philippines, and the subtropical region (122°–160°E, 20°–33°N). CPL_KF shows overall cold biases over these regions (Fig. 3d), while CPL_EM and CPL_Tie exhibit warm biases over east of the Philippines, with further eastward extension in CPL_Tie (Fig. 3c). In addition, CPL_EM shows larger cold (warm) biases over the subtropical region (southern South China Sea) than CPL_Tie.

Figure 4a shows the probability density function (PDF) distribution of simulated SST biases over WNP from three regionally coupled simulations. Consistent with Fig. 3d, a dominant cold bias is found in the CPL_KF simulation with a peak around − 0.63 °C. An overall normal mode type of distribution is found in both CPL_EM and CPL_Tie with a slightly larger frequency of warm bias for CPL_Tie. Quantitatively, 48.3% (44.8%) of the model grids have biases within ± 0.5 °C in CPL_Tie (CPL_EM), while the percentage is 39.5% for CPL_KF. These results demonstrate that the regionally coupled simulation with the Tiedtke scheme exhibits a comparable performance to the MIT-Emanuel scheme in the simulation of SST over WNP in the boreal summer, which is better than the simulation with the Kain–Frisch scheme.

To understand the reasons for the simulated SST biases, the sea surface energy budget for three key regions (shown in Fig. 3b) is analyzed. Table 1 shows the regional-averaged net solar radiation and longwave radiations fluxes, sensible and latent heat fluxes at the sea surface, derived from observations and regionally coupled simulations. In both observation and simulations, the solar radiation flux is the

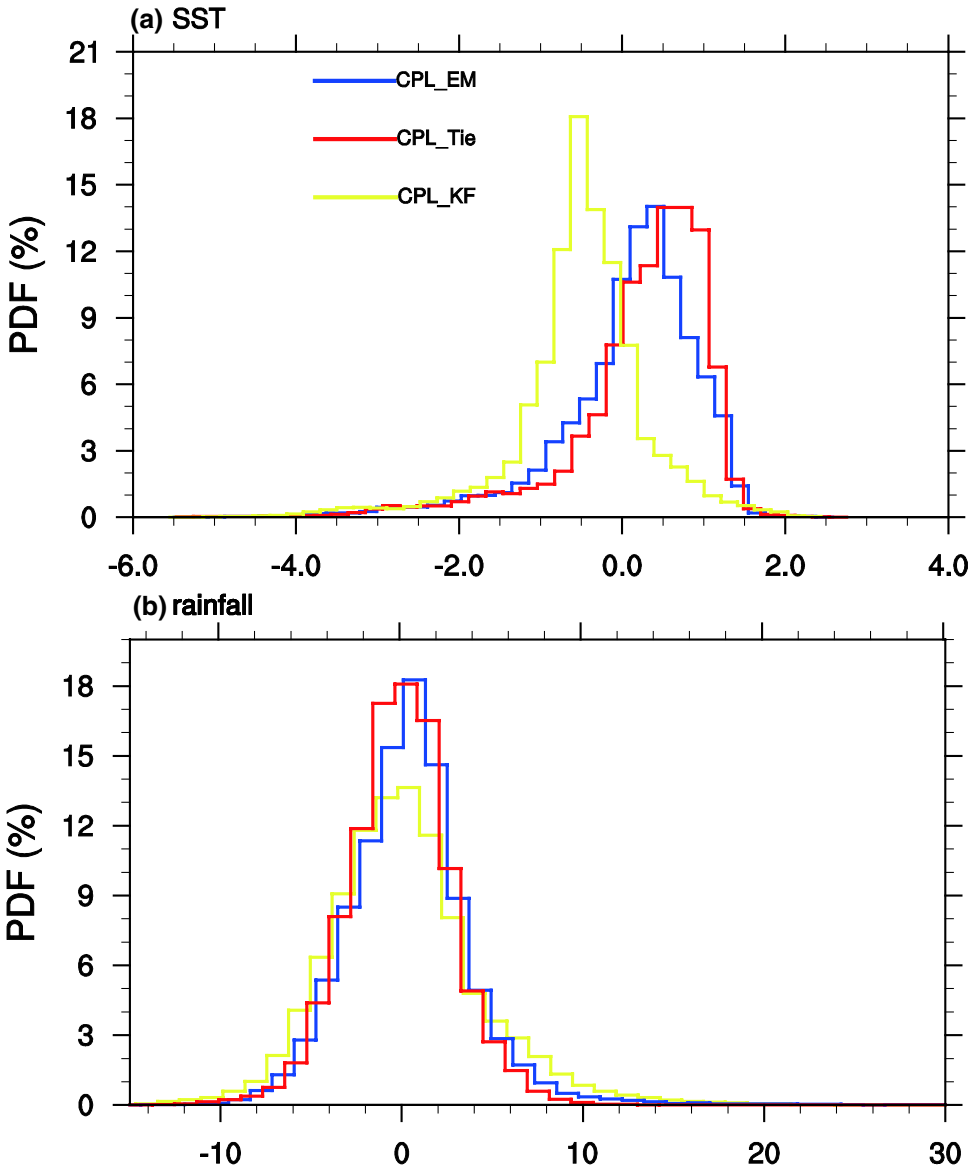

Fig. 4 The probability density function (PDF) distributions of simulated **a** SST biases (°C) and **b** rainfall biases (mm/day) over the WNP from the three regionally coupled simulations

most important component, while the latent heat flux is the second. Compared with the observations, the simulation with the Tiedtke scheme (CPL_Tie) gives the overall best estimation of sea surface heat budget.

It is evident that the cold biases of simulated SST in CPL_KF over the three regions are contributed mostly by the underestimation of the sea surface net solar radiation flux. Compared to CPL_EM, the slightly warmer SST over the east of the Philippines in CPL_Tie is associated with the larger sea surface net solar radiation flux, while the colder SST in CPL_EM over the subtropical region is primarily the result of the larger upward latent heat flux and the longwave radiation flux.

3.2 Rainfall and circulation simulations

Figure 5 shows the spatial distribution of the precipitation, averaged from June to August of 2005, from observation and regionally coupled simulations. The observed precipitation (Fig. 5a) is characterized by the major rainbands over the monsoon trough located over east of the Philippines (Region 1), the northern South China Sea (Region 2), the region extending northeast from southern China to the east of Japan (Region 3), and the Mei-yu front region from Yangtze–Huai River Valley to the Korean Peninsula (Region 4). The rainfall center over the northern South China Sea is reasonably reproduced in all three simulations, while those over southern China and the Yangtze–Huai River Valley are underestimated in all the simulations. However, the simulated rainfall over the monsoon trough varies with different cumulus

Table 1 Observed and simulated net solar radiation (SD), longwave radiation (LW) sensible heat (SH) and latent heat (LH) fluxes at the sea surface averaged from June to August 2005 for the three regions shown in Fig. 3b

	Observation	CPL_EM	CPL_Tie	CPL_KF
1. South China Sea				
SD	203.7	198.5	197.0	152.0
LW	45.7	44.7	43.4	32.4
SH	6.1	2.1	8.3	– 2.6
LH	108.4	126.1	113.0	84.0
2. East of the Philippines				
SD	210.6	188.1	197.2	122.7
LW	48.7	42.4	43.3	26.5
SH	8.7	4.5	13.5	– 2.1
LH	113.7	108.7	105.7	88.8
3. Subtropical region				
SD	241.7	230.6	232.4	205.0
LW	45.8	48.4	44.7	41.1
SH	1.1	0.4	6.5	– 0.8
LH	85.8	91.7	88.5	73.3

The observed radiation fluxes (turbulence fluxes) are from CERES (OAFlux) data. Units: W/m^2

parameterization schemes. Among the three simulations, the CPL_Tie simulation reasonably captures the shape and magnitude of the monsoon trough rainfall, while the CPL_EM (CPL_KF) simulation tends to underestimate (overestimate) the rainfall. This is supported by a higher SCC of 0.62 for CPL_Tie, while it is 0.40 (0.52) for CPL_EM (CPL_KF). The deficiency of the CPL_Tie simulation is it exhibits less small-scale features than the other simulations.

The PDFs of JJA-mean rainfall biases over WNP are shown in Fig. 4b. Normal model type distributions of biases are evident for all three simulations, but the percentages of the model grids with rainfall biases of approximately zero in the CPL_KF simulation are much lower than those in the CPL_EM and CPL_Tie simulations. Quantitatively, 51.9% (48.2%) of the model grids have rainfall biases within ± 2 mm/day in CPL_Tie (CPL_EM), while the percentage is 38.4% for the CPL_KF simulation. These results highlight the improved performance of the summer rainfall simulation over WNP with the Tiedtke scheme than those with the MIT-Emanuel and Kain–Fritsch schemes in our regionally coupled simulations.

Figure 6 compares the performances of the models in the simulation of geopotential height at 500 hPa and low-level wind at 850 hPa averaged from June to August of 2005. In the observation (Fig. 6a), the western North Pacific

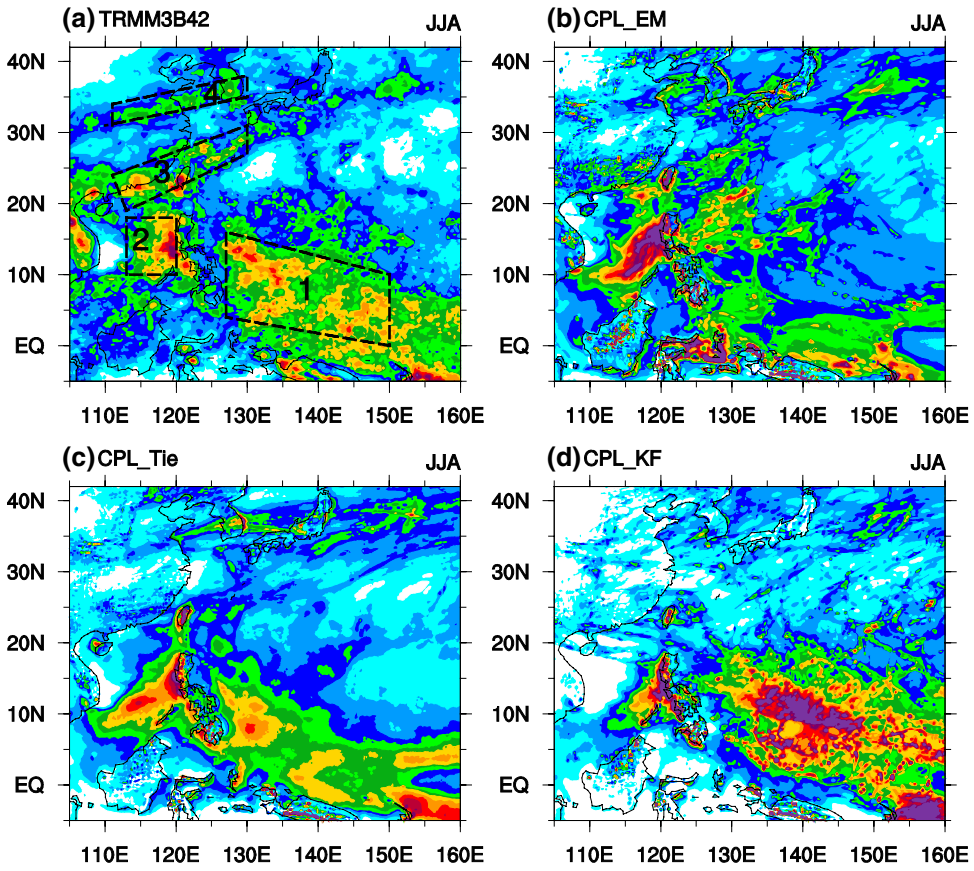

Fig. 5 Spatial distributions of precipitation (mm/day) averaged from June to August 2005 over the WNP derived from **a** observation, **b** CPL_EM, **c** CPL_Tie, and **d** CPL_KF. The four regions (numbers 1–4) in **a** illustrate the locations of the observed major rainband/centers

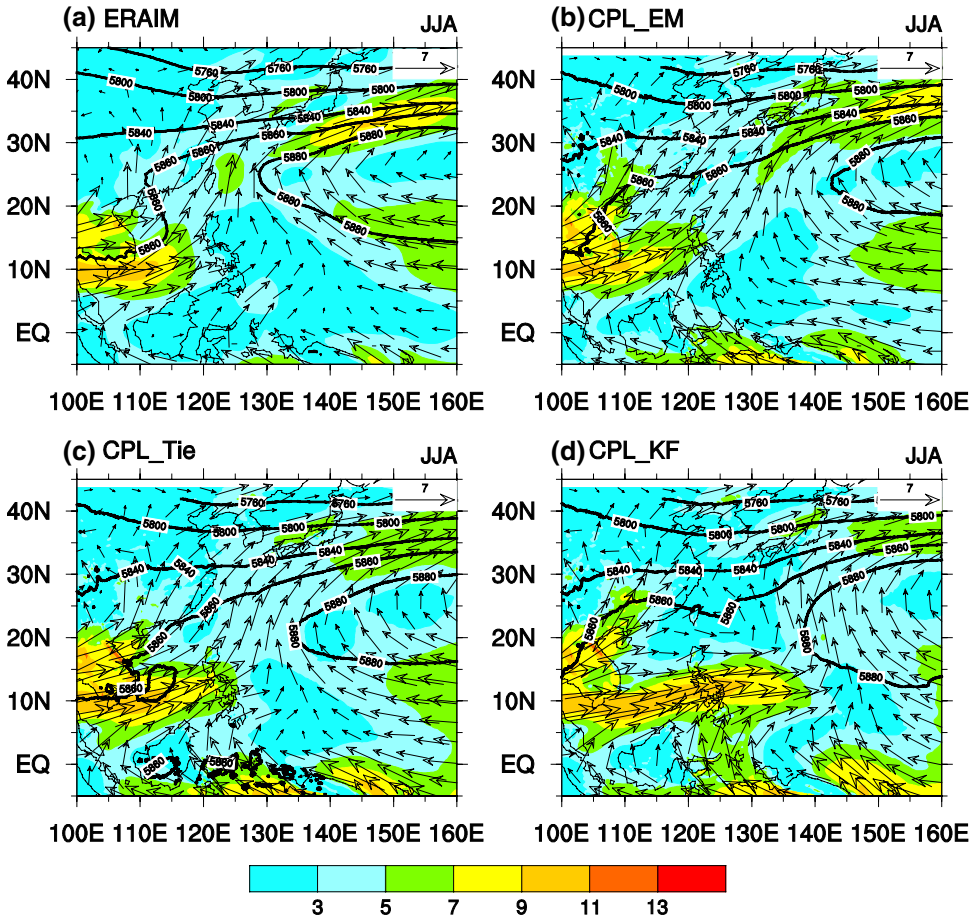

Fig. 6 Spatial distributions of the geopotential height at 500 hPa (contour, gpm), the low-level wind at 850 hPa (vector, m/s) and the corresponding wind speed (shading, m/s) averaged from June to August 2005 over the WNP derived from **a** observation, **b** CPL_EM, **c** CPL_Tie, and **d** CPL_KF

subtropical high (WNPSH) is the major system over WNP. The low-level westerly wind associated with the Indian summer monsoon, the cross-equatorial flow passing across the Maritime Continent, and the low-level southeasterly associated with the WNPSH converge over east of the Philippines. The general pattern of the WNPSH and the associated low-level wind is captured by each simulation, although some differences are still found. The simulated WNPSH is weaker and shifts eastward compared with the observation. However, among the three simulations, the western ridge of the WNPSH that was simulated by CPL_Tie most resembles the observation (Fig. 6c). Another major deficiency of CPL_KF is that the simulated low-level westerly wind associated with the Indian summer monsoon extends too far eastward to the Philippine Sea, which favors the eastward shift of the monsoon trough (Fig. 5d).

To quantitatively evaluate the models' performances, Fig. 7 shows the Taylor diagram illustrating the relative mean squared difference and the SCC between the simulations and the observations for SST, rainfall and circulation fields. It is well known that the model tends to better reproduce the large scale variables (SST and circulation fields) than regional scale variables (such as rainfall). The CPL_Tie simulation better captures the spatial pattern of

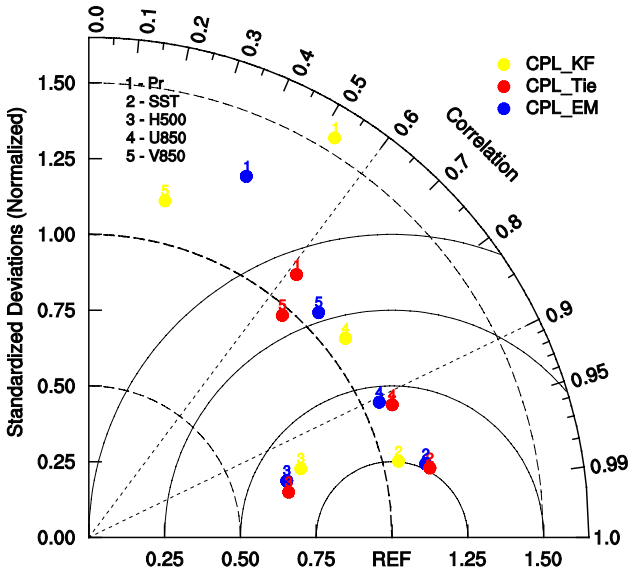

Fig. 7 Taylor diagram evaluating simulations of the SST, precipitation (Pr), geopotential height at 500 hPa (H500), horizontal (U850) and meridional (V850) winds at 850 hPa over the WNP. The angular coordinate is the correlation coefficients between model results and the observations. The radial coordinate is the standard deviation of model results divided by the standard deviation of the observations

those essential climate variables over WNP than the other two simulations as evidenced by the higher SCCs (Fig. 7). The distance between each variable and the reference point marked "REF" on the horizontal axis measures the RMSE, which can be used to quantify how closely the simulation matches the observation. In terms of RMSE, although no significant difference is found for some variables (SST and geopotential height at 500 hPa) among the three simulations, it is evident that the CPL_Tie simulation exhibits the smallest RMSE for rainfall that may be the most important variable for this region.

The WNPSH is a major circulation system that governs the time evolution of rainfall over this region (Tao and Chen 1987). Figure 8 shows the time–latitude cross section of the rainfall and the 5860 gpm, which is used to roughly represent the position of WNPSH averaged between 110°E and 130°E from May 1 to August 31, 2005. A 5-day running average was applied to the geopotential height for both observation and simulations. In the observation (Fig. 8a), the rainband propagates northward from approximately 15°N in early June to approximately 35°N in early July and then retreats southward to approximately 13°N in later July, thereafter remaining quasi-stationary until mid-August. This propagation of the rainband closely follows the movement of the WNPSH. The propagation of the rainband simulated by CPL_Tie is comparable to that simulated by CPL_EM as evidenced by the SCC of 0.39 vs. 0.37, while it is better than that simulated by CPL_KF, with a SCC of 0.20. The northward movement of the rainband is reasonably reproduced by both the CPL_EM and CPL_Tie simulations (Fig. 8b, c); however, it is too weak in the CPL_KF simulation and does not jump as far north as it does in the observation (Fig. 8d).

3.3 Moisture flux

Water vapor transport is one of the most important components of the western North summer monsoon system, which plays a crucial role in determining the major rainband. The vertically integrated moisture flux convergence is defined as $-\left\langle \nabla \cdot \left(\vec{V}q\right)\right\rangle$, where $\vec{V}$ and q are wind vectors and specific humidity, respectively. The triangle parenthesis indicates a vertical integration from the surface to the tropopause. ∇ is the gradient operator. The total vertically integrated moisture flux convergence can be decomposed into two terms, as shown below:

$$-\left\langle \nabla \cdot \left(\vec{V}q\right)\right\rangle = -\left\langle \omega \partial_p q\right\rangle - \left\langle u\partial_x q + v\partial_y q\right\rangle \quad (1)$$

The right-hand terms of Eq. (1) denote vertical moisture advection including the horizontal moisture convergence, and horizontal moisture advection, respectively.

Figure 9 shows the observed and simulated vertically integrated moisture flux convergence, vertical moisture advection, and horizontal moisture advection along with the

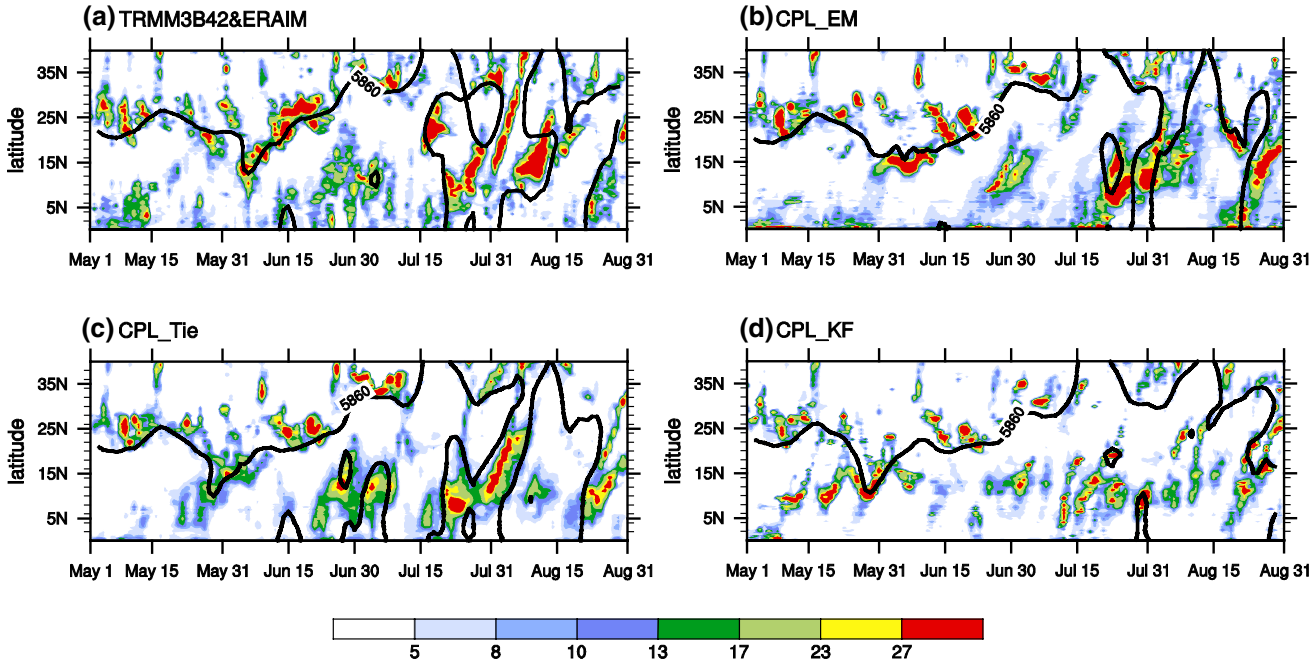

Fig. 8 The time–latitude cross sections of the rainfall (shading, mm/day) and the 5860 gpm (contour) averaged between 110°E and 130°E from May 1 to August 31, 2005 derived from **a** observation, **b** CPL_EM, **c** CPL_Tie, and **d** CPL_KF. A 5-day running average was applied to the geopotential height from both observation and simulations

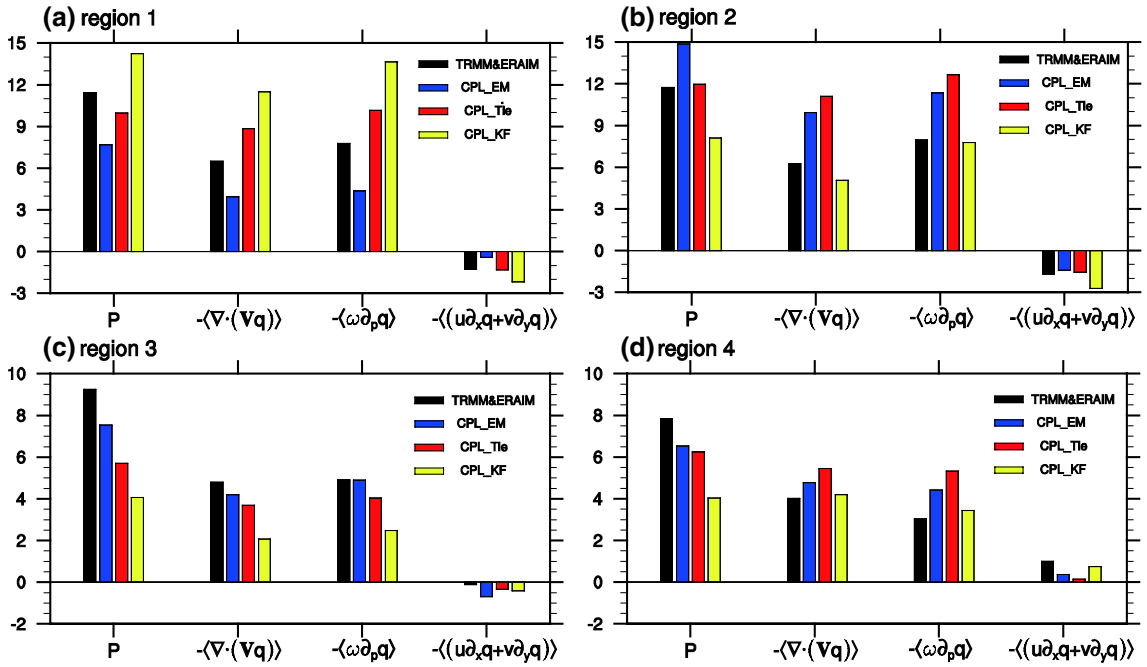

Fig. 9 The vertically integrated moisture flux convergence $\left(-\left\langle \nabla \cdot \left(\vec{V}q\right)\right\rangle, \mathrm{mm/day}\right)$, vertical moisture advection $\left(-\left\langle \omega \partial_p q\right\rangle, \mathrm{mm/day}\right)$, horizontal moisture advection $\left(-\left\langle u\partial_x q + v\partial_y q\right\rangle, \mathrm{mm/day}\right)$ and precipitation (mm/day) averaged over **a** Region 1, **b** Region 2, **c** Region 3, and **d** Region 4. The four regions are shown as boxes in Fig. 5a

precipitation averaged over four major rain bands (shown in Fig. 5a). In the observation, the vertically integrated moisture flux convergence contributes approximately 53% of the rainfall formation. The vertical moisture advection is the dominant term due to the weak horizontal gradient of moisture in the tropics. The horizontal moisture advection contributes negatively to the rainfall formation except over the Meiyu front region (Fig. 9d). The contribution by the horizontal moisture advection is well captured by all the simulations; however, all the simulations overestimate the percentages of the contribution of the moisture flux convergence to the simulated rainfall. In Region 1 and Region 3, the simulated rainfall biases are generally in line with the biases of vertical moisture advection; that is, the simulation that underestimates (overestimates) the vertical moisture advection tends to have dry (wet) biases. However, this relationship is not true for Regions 2 and 4, implying that surface evaporation may also contribute to the rainfall biases.

4 Discussion

One of the major differences among the three regionally coupled simulations is the simulated rainfall over the monsoon trough. Only the simulation with the Tiedtke scheme well captures the shape and magnitude of the rainband, while that with the MIT-Emanuel (Kain–Fritsch) scheme tends to underestimate (overestimate) the rainfall there. In this section, we will explore the underlying reasons.

The cumulus parameterization has significant impacts on the diabatic heating profile of the model (Yanai et al. 1973). Here, we calculate the atmospheric apparent heat source (Q_1) and apparent moisture sink (Q_2) according to Yanai et al. (1973):

$$Q_1 = c_p \frac{\partial T}{\partial t} - c_p \left(\omega \frac{RT}{c_p p} - \omega \frac{\partial T}{\partial p} - \mathrm{V} \cdot \nabla T \right), \tag{2}$$

$$Q_2 = -L \frac{\partial q}{\partial t} - L\mathrm{V} \cdot \nabla q - L\omega \frac{\partial q}{\partial p} \tag{3}$$

where c_p is the specific heat at constant pressure, T is the temperature, ω is the vertical p velocity, R is the gas constant, V is the horizontal velocity vector, L is the latent heat of condensation, and q is the specific humidity. Q_1 represents the total diabatic heating, while Q_2 represents the latent heating associated with the condensation or evaporation processes.

Figure 10 shows the vertical profile of Q_1 and Q_2 fields averaged over the monsoon trough (Region 1 in Fig. 5a) for the summer mean of 2005. In the observation, the vertical profile of Q_2 shows a maximum rate on the order

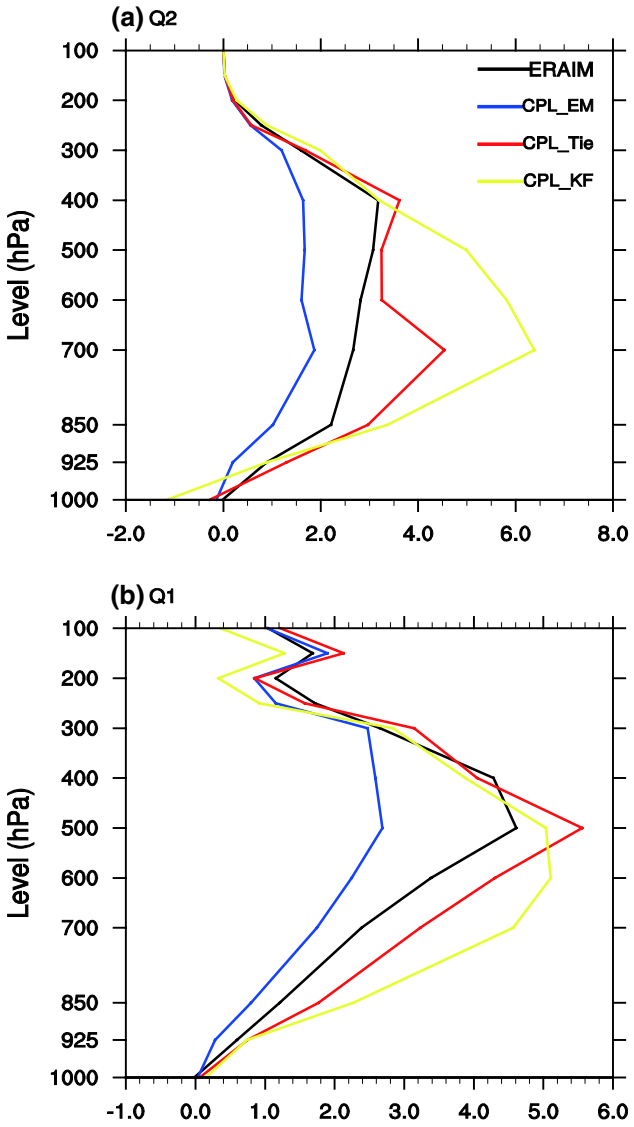

Fig. 10 The vertical profiles of the apparent moisture sink (Q_2/C_P, °C/day) and heat source (Q_1/C_P, °C/day) fields averaged over the monsoon trough (Region 1 in Fig. 5a) for the summer mean of 2005 and derived from observation and simulations

of 3 K/day at approximately 400–500 hPa (Fig. 10a). Although all of the simulated Q_2 fields exhibit a peak at approximately 700 hPa, a second peak is found at approximately 400 hPa in the CPL_Tie simulation. More significantly, the vertically integrated Q_2 simulated by CPL_Tie is comparable to observation, while that simulated by the CPL_EM (CPL_KF) is nearly half (double) the observed counterpart.

The observed total diabatic heating Q_1 (Fig. 10b) has a similar vertical distribution to Q_2, but with an enhanced peak at approximately 500 hPa. Again, the vertical distribution of the observed Q_1 is reasonably simulated by the CPL_Tie simulation, despite slightly larger amplitude in the middle and lower troposphere. As with the simulated Q_2, the Q_1 simulated by CPL_EM is much weaker than the observation. Although the amplitude of the simulated Q_1 in CPL_KF is reduced compared to the simulated Q_2, the simulated diabatic heating rate is still double the observed in the lower troposphere.

The diabatic heating and the vertical motion are closely related. Figure 11 shows the longitude–height cross sections of observed and simulated vertical p velocity, averaged between 2°N and 18°N for the summer mean of 2005. Followed by the too weak diabatic heating simulated by CPL_EM (Fig. 10b), the simulated ascending motion over the monsoon trough (from 125°E to 150°E) is much weaker than the observation (Fig. 11b), which results in the underestimation of the vertical moisture advection (Fig. 9b). In contrast, accompanied by the much stronger-than-the observed diabatic heating, the simulated ascending motion by CPL_KF is significantly overestimated, especially in the lower troposphere, and extends farther eastward, which leads to a much stronger vertical moisture advection (Fig. 9d). The vertical distribution and the magnitude of vertical motion are reasonably reproduced in the CPL_Tie simulation but with a slight overestimation (Fig. 11c), which is associated with the relatively well-simulated diabatic heating profile.

Figure 12 further shows the vertical profiles from the simulations of the regional averaged cloud liquid water path and cloud fractional cover over the monsoon trough for the summer mean of 2005. A direct comparison with the observation is not available since the cloud simulator has not been introduced in the RegCM4 used in this study. As expected, the cloud liquid water path and cloud fractional cover simulated by CPL_KF are much larger than for the other two simulations in the middle and lower troposphere, which is associated with the overestimated convective condensation (Fig. 10a). This causes the large reduction in the solar radiation that reaches the sea surface, which favors the cold biases of SST there (Fig. 3d). However, compared to those simulated by CPL_Tie, less (more) cloud liquid water path and cloud fractional cover are simulated by CPL_EM in the lower (upper) troposphere. This may explain the comparable simulated sea surface solar radiation flux and the resulting SST biases in the CPL_EM and CPL_Tie simulations (Fig. 3).

To further discuss the behavior of different cumulus schemes, Fig. 13 shows the scatter plots of the regional averaged convective available potential energy (CAPE) and the precipitation over the monsoon trough from June 1 to August 31 of 2005. Over the monsoon trough, the precipitation and CAPE are negatively correlated (Fig. 13a), with a correlation of − 0.42. Since the CAPE strongly depends on the boundary layer equivalent potential temperature, which is mainly affected by the surface heat and moisture fluxes (Zhang 2003), this negative correlation

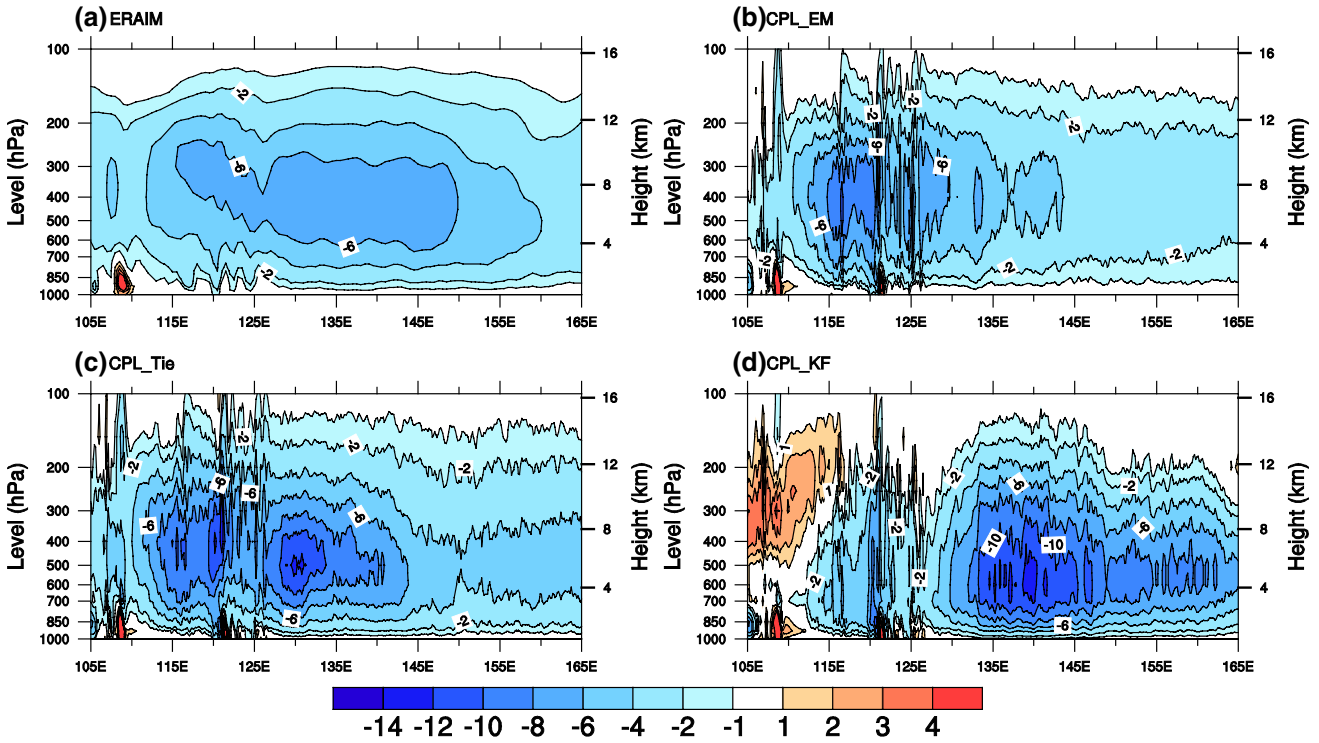

Fig. 11 The longitude–height cross sections of vertical *p* velocity (100 hPa/s) averaged between 2°N and 18°N for the summer mean of 2005 derived from **a** observation, **b** CPL_EM, **c** CPL_Tie, and **d** CPL_KF

suggests that the precipitation/convection over the monsoon trough is more closely tied to the tropospheric large-scale forcing rather than the boundary layer forcing. In CPL_EM, however, the CAPE is positively correlated with the precipitation (Fig. 13b), because the convection in the MIT-Emanuel cumulus scheme is mainly driven by the buoyancy and does not take into account the effects of the large-scale environment (Chow et al. 2006). This negative correlation is partly reproduced in both CPL_Tie (Fig. 13c) and CPL_KF (Fig. 13d) with improved performance in CPL_Tie (Fig. 13c), possibly because some large scale forcings, i.e., large-scale moist convergent flow in the Tiedtke scheme or grid scale vertical motion in the Kain–Fritsch scheme have been taken into account.

The simulated precipitation over the monsoon trough in CPL_KF exhibits too strong a response to the low-level vertical velocity. Figure 14 shows the scatter plots of the regional averaged low-level vertical velocity at 925 hPa and the precipitation over the monsoon trough from June 1 to August 31 of 2005. In the observation, the precipitation over the monsoon trough is positively correlated with the vertical velocity at 925 hPa, with a correlation of 0.65 (Fig. 14a). This relationship is reasonably simulated by the CPL_EM and CPL_Tie; however, this correlation is much higher in CPL_KF (0.96; Fig. 14d).

In summary, the better performance over the monsoon trough in CPL_Tie could be attributed to at least three factors: (1) the improved simulated vertical profile of diabatic heating; (2) the inclusion of the effects of large-scale forcing in the cumulus parameterization; and (3) the reasonable simulated relationship with the low-level vertical velocity.

5 Summary and concluding remarks

5.1 Summary

In this study, we developed a high-resolution regional ocean–atmosphere coupled model based on RegCM4 and a North Pacific Ocean model. The horizontal resolution of the atmospheric component was set to 15 km, while that of the oceanic component was 0.1°. This regionally coupled model was applied to the western North Pacific region for a 1-year simulation from Nov. 2004 through Nov. 2005. The sensitivity of the regional ocean–atmosphere coupled model to three cumulus parameterization schemes (MIT-Emanuel,

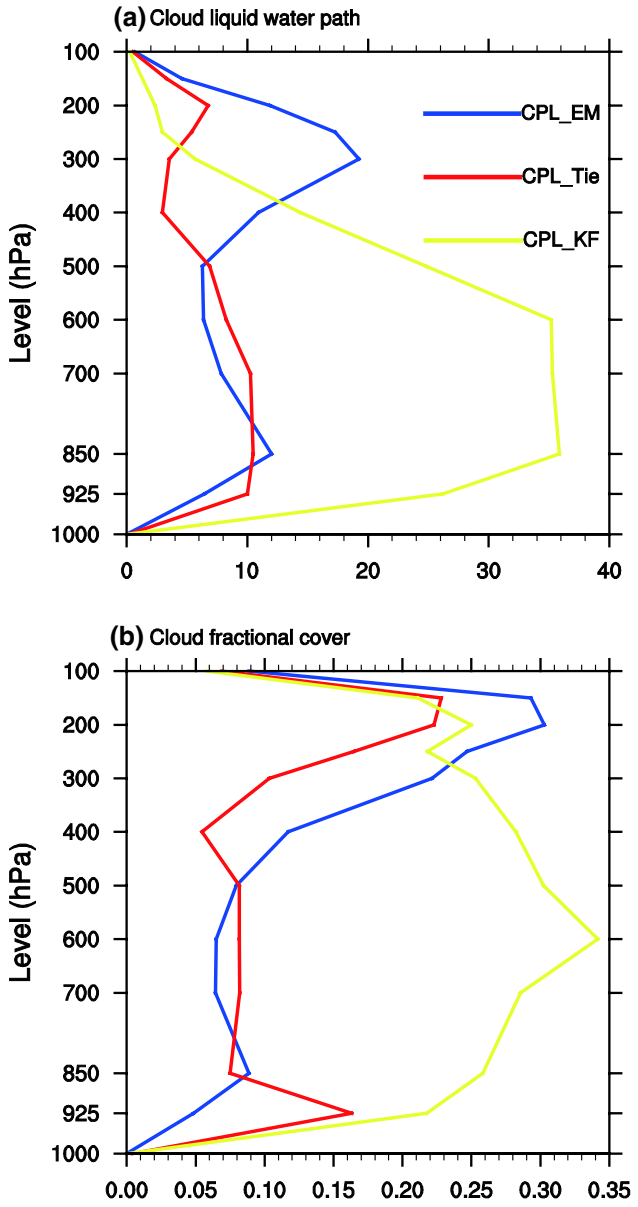

Fig. 12 Vertical profiles of the regional averaged **a** cloud liquid water path (g/m^2) and **b** cloud fractional cover over the monsoon trough for the summer mean of 2005 from the simulations

Tiedtke, Kain–Fritsch) was investigated with a focus on the western North Pacific summer monsoon. The underlying mechanisms were also discussed. The major results are summarized below.

1. The spatial pattern of the observed SST in the boreal summer of 2005 is reasonably captured by each simulation; however, overall cold biases are found in the CPL_KF scheme followed by the significant underestimation of sea surface solar radiation flux. Nearly 50% of the model grids have biases within ± 0.5 °C in CPL_EM and CPL_Tie, while the percentage is approximately 40% in CPL_KF.
2. The general pattern of the western North Pacific subtropical high (WNPSH) and the associated low-level wind is captured by each simulation; however, the western ridge of the WNPSH simulated by CPL_Tie most closely resembles the observation. For the summer mean precipitation, 51.9% (48.2%) of the model grids have rainfall biases within ± 2 mm/day in CPL_Tie (CPL_EM), while the percentage is 38.4% for CPL_KF. In particular, the spatial pattern of the observed precipitation is well captured by CPL_Tie, especially over the monsoon trough, while CPL_EM (CPL_KF) tends to underestimate (overestimate) the rainfall over the monsoon trough. The propagation of the simulated rainband and the associated WNPSH is also well captured by CPL_Tie.
3. The vertical profiles of the apparent heat source and moisture sink over the monsoon trough simulated by CPL_Tie are comparable to those of the observation, while those simulated by CPL_EM (CPL_KF) are nearly half (double) of those observed, especially over the lower troposphere. The too weak (strong) diabatic heating simulated by CPL_EM (CPL_KF) favors a weaker (stronger) ascending motion and then leads to the underestimation (overestimation) of vertical moisture advection over the monsoon trough.
4. The precipitation/convection over the monsoon trough is more closely tied to the tropospheric large-scale forcing than the boundary layer forcing. The deficiencies of CPL_EM over the monsoon trough are partly because the convection in the MIT-Emanuel cumulus scheme is mainly driven by the buoyancy and does not take into account the effects of the large-scale environment, whereas the deficiency of CPL_KF may be attributed to the too strong response of precipitation to the low-level vertical velocity.

5.2 Concluding remarks

The current conclusions are based on the case study of the year 2005, when the WNPSM is normal. To examine whether the conclusions are case-dependent, we have conducted another case simulations for the year 2004. The summer of 2004 is an extreme case with a strong WNPSM (Wang et al. 2008). Similar to the case of 2005, the regionally coupled simulation with the Tiedtke scheme exhibits relatively better performances over this region for the case of 2004 in terms of the SST and precipitation (figures not shown). The performance of the developed regional

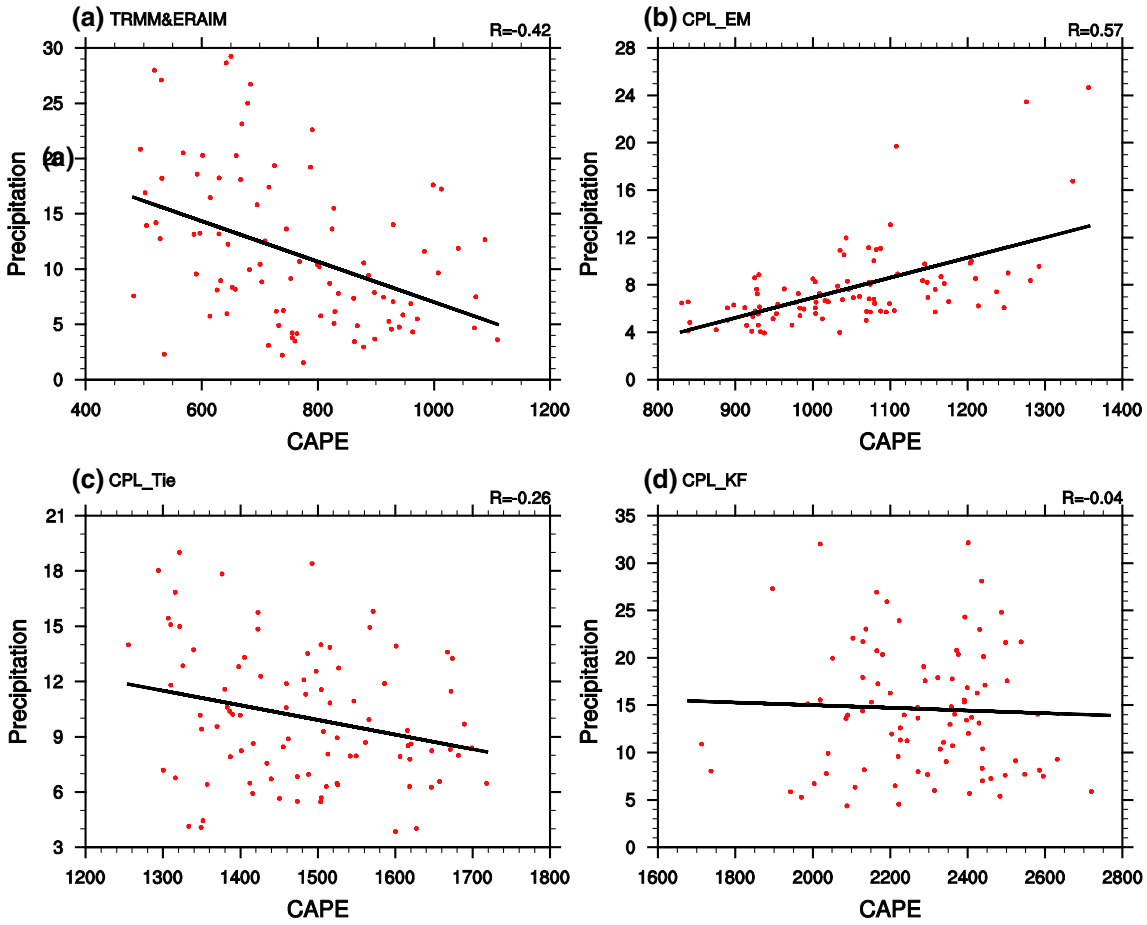

Fig. 13 Scatter plots of the regional averaged convective available potential energy (CAPE, J/kg) and the precipitation (mm/day) over the monsoon trough from June 1 to August 31 2005 from **a** observation, **b** CPL_EM, **c** CPL_Tie, and **d** CPL_KF. The correlation coefficients are shown at the top-right corner of each plot

ocean–atmosphere coupled model in the simulation of the interannual variability of East Asian-western North Pacific monsoon deserves further study.

In addition, the sensitivity to the cumulus parameterization schemes may be altered for a different horizontal resolution, since the three cumulus parameterization schemes used in this study are not scale-awareness schemes. The simulation with the Tiedtke scheme also exhibits some biases, i.e., lacks of small-scale features in precipitation, overestimation of convective percentages (figure not shown). It is noticed that some parameters such as the parameters related to the entrainment/detrainment rates in the Tiedtke scheme are tunable. Li et al. (2007) tuned the Tiedtke scheme for an atmospheric general circulation model. They increased the entrainment–detrainment coefficient for shallow convection and penetrative convection, introduced a relative humidity trigger and reduced the autoconversion parameter. Then, the simulated convective rainfall was reduced in the tropics. Therefore, the performance of the regional coupled model may be better by calibrating the key physical parameters and warrants further investigation.

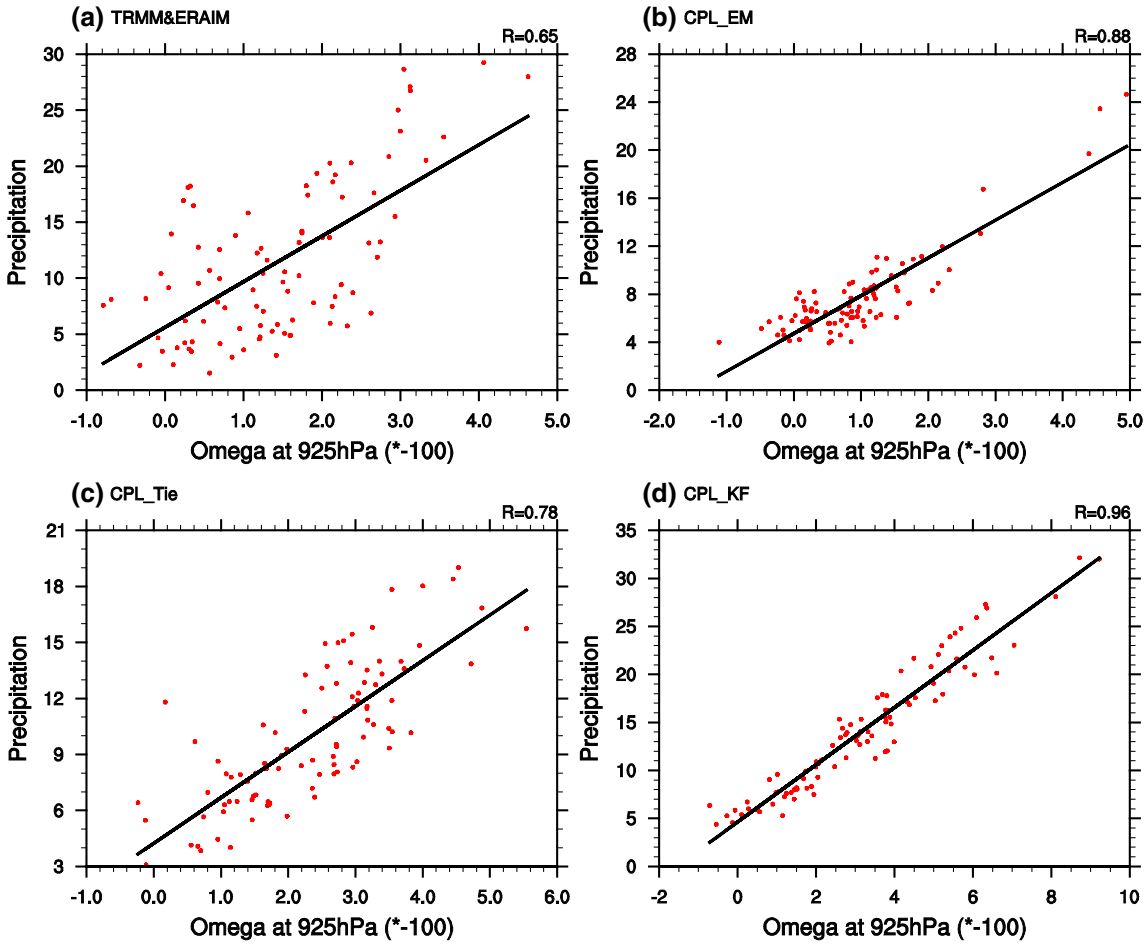

Fig. 14 Scatter plots of the regional averaged vertical p velocity (omega, − 100 hPa/s) and the precipitation (mm/day) over the monsoon trough from June 1 to August 31, 2005 from **a** observation, **b** CPL_EM, **c** CPL_Tie, and **d** CPL_KF. The correlation coefficients are shown at the top-right corner of each plot

Acknowledgements This work was jointly supported by the National Key Research and Development Program of China (2018YFA0606003), the National Natural Science Foundation of China (Grants 41875132, 41575105, 41776030), and the Jiangsu Collaborative Innovation Center for Climate Change.

References

Antonov JI, Locarnini RA, Boyer TP, Mishonov AV, Garcia HE (2006) World Ocean Atlas 2005, Volume 2: Salinity. In: Levitus S (ed) NOAA Atlas NESDIS 62. US Government Printing Office, Washington, D.C., p 182

Bao Q, Lin P, Zhou T, Liu Y, Yu Y, Wu G, He B, He J, Li L, Li J, Li Y, Liu H, Qiao F, Song Z, Wang B, Wang J, Wang P, Wang X, Wang Z, Wu B, Wu T, Xu Y, Yu H, Zhao W, Zheng W, Zhou L (2013) The flexible global ocean–atmosphere–land system model, spectral version 2: FGOALS-s2. Adv Atmos Sci 30:561–576

Canuto VM, Howard A, Cheng Y, Dubovikov MS (2001) Ocean turbulence. Part I: one-point closure model-momentum and heat vertical diffusivities. J Phys Oceanogr 31:1413–1426

Canuto VM, Howard A, Cheng Y, Dubovikov MS (2002) Ocean turbulence. Part II: vertical diffusivities of momentum, heat, salt, mass, and passive scalars. J Phys Oceanogr 32:240–264

Cha D-H, Jin CS, Moon JH, Lee DK (2016) Improvement of regional climate simulation of East Asian summer monsoon by coupled air–sea interaction and large-scale nudging. Int J Climatol 36:334–345. https://doi.org/10.1002/joc.4349

Chelton DB, Schlax MG, Freilich MH, Milliff RF (2004) Satellite measurements reveal persistent small-scale features in ocean winds. Science 303:978–983

Chow KC, Chan JCL, Pal JS, Giorgi F (2006) Convection suppression criteria applied to the MIT cumulus parameterization scheme for simulating the Asian summer monsoon. Geophys Res Lett 33:L24709. https://doi.org/10.1029/2006GL028026

Christensen JH, Hewitson B, Busuioc A, Chen A, Gao X, Held R, Jones R, Kolli RK, Kwon WK, Laprise R, Magana Rueda V, Mearns L, Menendez CG, Räisänen J, Rinke A, Sarr A, Whetton P, Arritt R, Benestad R, Beniston M, Bromwich D, Caya D, Comiso J, de Elia R, Dethloff K (2007) Regional climate projections. In: Solomon S (ed) Climate change 2007: the physical science basis. Cambridge University Press, Cambridge, pp 847–940

Dai Y, Li H, Sun L (2018) The simulation of East Asian summer monsoon precipitation with a regional ocean–atmosphere coupled model. J Geophys Res Atmos. https://doi.org/10.1029/2018JD028541

Dee DP, Uppala SM, Simmons AJ, Berrisford P, Poli P, Kobayashi S, Andrae U, Balmaseda MA, Balsamo G, Bauer P, Bechtold P, Beljaars ACM, van den Berg L, Bidlot J, Bormann N, Delsol C, Dragani R, Fuentes M, Geer AJ, Haimberger L, Healy SB, Hersbach H, Holm EV, Isaksen L, Kallberg P, Kohler M, Matricardi M, McNally AP, Monge-Sanz BM, Morcrette J-J, Park B-K, Peubey C, de Rosnay P, Tavolato C, Thepaut J-N, Vitart F (2011) The ERA-Interim reanalysis: configuration and performance of the data assimilation system. Q J R Meteorol Soc 137:553–597. https://doi.org/10.1002/qj.828

Emanuel KA (1991) A scheme for representing cumulus convection in large-scale models. J Atmos Sci 48:2313–2335

Emanuel KA, Rothman MZ (1999) Development and evaluation of a convection scheme for use in climate models. J Atmos Sci 56:1766–1782

Gao XJ, Shi Y, Giorgi F (2016) Comparison of convective parameterizations in RegCM4 experiments over China with CLM as the land surface model. Atmos Ocean Sci Lett 9(4):246–254

Giorgi F, Mearns LO (1999) Introduction to special section: regional climate modeling revisited. J Geophys Res 104:6335–6352

Giorgi F, Jones C, Asrar GR (2009) Addressing climate information needs at the regional level: the CORDEX framework. WMO Bull 58:175–183

Giorgi F, Coppola E, Solmon F, Mariotti L, Sylla MB, Bi X, Elguindi N, Diro GT, Nair V, Giuliani G, Turuncoglu UU, Cozzini S, Guttler I, O'Brien TA, Tawfik AB, Shalaby A, Zakey AS, Steiner AL, Stordal F, Sloan LC, Brankovic C (2012) RegCM4: model description and preliminary test over multiple CORDEX domains. Clim Res 52:7–29

Giorgi F, Torma C, Coppola E, Ban N, Schar C, Somot S (2016) Enhanced summer convective rainfall at Alpine high elevations in response to climate warming. Nat Geosci 9:584–590

Gutowski WJ Jr, Giorgi F, Timbal B et al (2016) WCRP COordinated Regional Downscaling EXperiment (CORDEX): a diagnostic MIP for CMIP6. Geosci Model Dev 9:4087–4095

Holtslag AAM, de Bruijn EIF, Pan H-L (1990) A high resolution air mass transformation model for short-range weather forecasting. Mon Weather Rev 118:1561–1575

Jones C, Giorgi F, Asrar G (2011) The coordinated regional downscaling experiment: CORDEX an international downscaling link to CMIP. CLIVAR Exch 16(2):34–40

Kain JS (2004) The Kain–Fritsch convective parameterization: an update. J Appl Meteorol 43:170–181

Kain JS, Fritsch JM (1993) Convective parameterization for mesoscale models: the Kain–Fritcsh scheme. In: Emanuel KA, Raymond DJ (eds) The representation of cumulus convection in numerical models. American Meteor Society, Boston, p 246

Kiehl JT, Hack JJ, Bonan GB, Boville BA, Breigleb BP, Williamson DL, Rasch PJ (1996) Description of the NCAR community climate model (CCM3), Tech. Rep. NCAR/TN-420 + STR, National Center for Atmospheric Research

Kumar KK, Hoerling M, Rajagopalan B (2005) Advancing dynamical prediction of Indian monsoon rainfall. Geophys Res Lett 32:L08704. https://doi.org/10.1029/2004GL021979

Leung LR, Mearns LO, Giorgi F, Wilby RL (2003) Regional climate research—needs and opportunities. Bull Am Meteorol Soc 84:89–95

Li T, Zhou G (2010) Preliminary results of a regional air–sea coupled model over East Asia. Chin Sci Bull 55:1. https://doi.org/10.1007/s11434-010-0071-0

Li L, Wang B, Wang Y, Wan H (2007) Improvements in climate simulation with modifications to the Tiedtke convective parameterization in the grid-point atmospheric model of IAP LASG (GAMIL). Adv Atmos Sci 24(2):323–335

Li L, Lin P, Yu Y, Wang B, Zhou T, Liu L, Liu H, Liu J, Bao Q, Xu S, Huang W, Xia K, Pu Y, Dong L, Shen S, Liu Y, Hu N, Liu M, Sun W, Shi X, Zheng W, Wu B, Song M, Liu H, Zhang X, Wu G, Xue W, Huang X, Yang G, Song Z, Qiao F (2013) The flexible global ocean–atmosphere–land system model: grid-point version 2: FGOALS-g2. Adv Atmos Sci 30:543–560. https://doi.org/10.1007/s00376-012-2140-6

Lin P, Liu H, MA J, Li Y (2019) Ocean mesoscale structure-induced air–sea interaction in a high-resolution coupled model. Atmos Ocean Sci Lett 12(2):98–106. https://doi.org/10.1080/16742834.2019.1569454

Liu H, Lin P, Yu Y, Zhang X (2012) The baseline evaluation of LASG/IAP Climate system Ocean Model (LICOM) version 2. Acta Meteorol Sin 26:318–329

Locarnini RA, Mishonov AV, Antonov JI, Boyer TP, Garcia HE (2006) World Ocean Atlas 2005, Volume 1: Temperature. In: Levitus S (ed) NOAA Atlas NESDIS 61. US Government Printing Office, Washington, DC, p 182

Lu SH, Chen YC, Zhu BC (2000) A coupled ocean model and atmosphere model and simulation experiment in the South China Sea area. Plateau Meteorol 19:415–426 **(in Chinese)**

Lui YS, Tam C-Y, Au-Yeung YM, Lau NG (2018) Role of cumulus parameterization on the seasonal and diurnal precipitation over Southeast Asia in RegCM4. Clim Dyn. https://doi.org/10.1007/s00382-018-4517-4

Luo J-J, Masson S, Roeckner E, Madec G, Yamagata T (2005) Reducing climatology bias in an ocean–atmosphere CGCM with improved coupling physics. J Clim 18:2344–2360

Ma X, Jing Z, Chang P et al (2016) Western boundary currents regulated by interaction between ocean eddies and the atmosphere. Nature. https://doi.org/10.1038/nature18640

Martinez-Castro D, Vichot-Liano A, Bezanilla-Morlot A, Centella-Artola A, Campbell J, Giorgi F, Viloria-Holguin CC (2018) The performance of RegCM4 over the Central America and Caribbean region using different cumulus parameterizations. Clim Dyn 50:4103–4126

Nordeng TE (1994) Extended versions of the convective parameterization scheme at ECMWF and their impact on the mean and transient activity of the model in the Tropics. ECMWF. TechMemo 206:41

Oleson K, Niu G, Yang Z, Lawrence D, Thornton P, Lawrence P et al (2008) Improvements to the Community Land Model and their impact on the hydrological cycle. J Geophys Res 113:G01021. https://doi.org/10.1029/2007JG000563

Pal JS, Small EE, Eltahir EAB (2000) Simulation of regional-scale water and energy budgets: representation of subgrid cloud and precipitation processes within RegCM. J Geophys Res 105(29):29579–29594

Raju PVS, Bhatla R, Almazroui M, Assiri M (2015) Performance of convection schemes on the simulation of summer monsoon features over the South Asia CORDEX domain using RegCM-4.3. Int J Climatol 35:4695–4706

Ratnam JV, Giorgi F, Kaginalkar A, Cozzini S (2009) Simulation of the Indian monsoon using the RegCM3–ROMS regional coupled model. Clim Dyn 33:119–139

Ren X, Qian Y (2005) A coupled regional air–sea model, its performance and climate drift in simulation of the East Asian summer monsoon in 1998. Int J Climatol 25:679–692

Reynolds RW, Smith TM, Liu C, Chelton DB, Casey KS, Schlax MG (2007) Daily high-resolution-blended analyses for sea surface temperature. J Clim 20:5473–5496

Seo H, Xie S-P, Murtugudde R, Jochum M, Miller AJ (2009) Seasonal effects of Indian Ocean freshwater forcing in a

regional coupled model. J Clim 22:6577–6596. https://doi.org/10.1175/2009JCLI2990.1
Tao SY, Chen LX (1987) A review of recent research on the east Asian summer monsoon in China. In: Chang CP, Krishnamurti TN (eds) Review of monsoon meteorology. Oxford University Press, New York, pp 60–92
Tiedtke M (1989) A comprehensive mass flux scheme for cumulus parameterization in large-scale models. Am Meteorol Soc 117:1779–1800
Valcke S (ed) (2006) OASIS3 User guide (prism_2-5). PRISM Support Initiative Report No.3, CERFACS, Toulouse, France
Wang Y, Leung LR, McGregor JL, Lee DK, Wang WC, Ding Y, Kimura F (2004) Regional climate modeling: progress, challenges, and prospects. J Meteorol Soc Jpn 82:1599–1628
Wang B, Ding Q, Fu X, Kang IS, Jin K, Shukla J, Doblas-Reyes F (2005) Fundamental challenge in simulation and prediction of summer monsoon rainfall. Geophy Res Lett 32:L15711. https://doi.org/10.1029/2005GL022734
Wang B, Wu Z, Li J, Liu J, Chang C-P, Ding Y, Wu G-X (2008) How to measure the strength of the East Asian summer monsoon? J Clim 21:4449–4463
Wielicki BA, Barkstrom BR, Harrison EF, Lee RB III, Louis SG, Cooper JE (1996) Clouds and the Earth's Radiant Energy System (CERES): an Earth observing system experiment. Bull Am Meteorol Soc 77:853–868
Yao S, Zhang Y (2010) Simulation of China summer precipitation using a regional air–sea coupled model. Acta Meteorol Sin 24:203–214
Yu L, Jin X, Weller R (2008) Multidecade global flux datasets from the objectively analyzed air–sea fluxes (OAFlux) project: latent and sensible heat fluxes, ocean evaporation, and related surface meteorological variables. Tech. Rep. OA-2008-01, Woods Hole Oceanographic Institution, p 64
Yu Y, Liu H, Lin P (2012) A quasi-global 1/10 eddy-resolving ocean general circulation model and its preliminary results. Chin Sci Bull 2012(57):3908–3916. https://doi.org/10.1007/s11434-012-5234-8
Zeng X, Zhao M, Dickinson RE (1998) Intercomparison of bulk aerodynamic algorithms for the computation of sea surface fluxes using TOGA COARE and TAO data. J Clim 11:2628–2644
Zhang GJ (2003) Roles of tropospheric and boundary layer forcing in the diurnal cycle of convection in the US southern great plains. Geophys Res Lett 30:2281. https://doi.org/10.1029/2003gl018554
Zhou T, Wu B, Wang B (2009) How well do Atmospheric General Circulation Models capture the leading modes of the interannual variability of Asian–Australian Monsoon? J Clim 22:1159–1173
Zou L, Zhou T (2011) Sensitivity of a regional ocean–atmosphere coupled model to convection parameterization over western North Pacific. J Geophys Res 116:D18106. https://doi.org/10.1029/2011JD015844
Zou L, Zhou T (2012) Development and evaluation of a regional ocean–atmosphere coupled model with focus on the western North Pacific summer monsoon simulation: impacts of different atmospheric components. Sci China Earth Sci 55:802–815
Zou L, Zhou T (2013) Can a regional ocean atmosphere coupled model improve the simulation of the interannual variability of the western North Pacific summer monsoon? J Clim 26:2353–2367
Zou L, Zhou T (2016) A regional ocean–atmosphere coupled model developed for CORDEX East Asia: assessment of Asian summer monsoon simulation. Clim Dyn 47:3627–3640. https://doi.org/10.1007/s00382-016-3032-8
Zou L, Zhou T, Peng D (2016) Dynamical downscaling of historical climate over CORDEX East Asia domain: a comparison of regional ocean atmosphere coupled model to standalone RCM simulations. J Geophys Res Atmos 121:1442–1458. https://doi.org/10.1002/2015JD023912